TITLE
ASP Conference Series, Vol. **VOLUME**, **PUBLICATION YEAR**
EDITORS

Detectable Signals from Mergers of Compact Stars

Hans-Thomas Janka

Max-Planck-Institut für Astrophysik, Karl-Schwarzschild-Str. 1, D-85741 Garching, Germany

Maximilian Ruffert

Department of Mathematics & Statistics, University of Edinburgh, Edinburgh, EH9 3JZ, Scotland, U.K.

Abstract. Merging neutron stars and neutron star–black holes binaries are powerful sources of gravitational waves. They have also been suggested as possible sources of cosmic gamma-ray bursts and are discussed as sites for the formation of r-process elements. Whereas the first aspect is undoubtable, the latter two are very uncertain. The current status of our knowledge and of the numerical modeling is briefly reviewed and the results of simulations are critically discussed concerning their significance and implications for potentially observable signals.

1. Introduction

Mergers of binary neutron stars (NS+NS) and neutron stars with companion black holes (NS+BH) are known to occur, because the emission of gravitational waves leads to a shrinking orbital separation and does not allow the systems to live forever. The Hulse-Taylor binary pulsar PSR B1913+16 (Hulse & Taylor 1975) is the most famous example among a handful of known systems (Thorsett & Chakrabarty 1999). Eventually, after 10^8–10^{10} years of evolution, these double stars will approach the final catastrophic plunge and will become powerful sources of gravitational radiation. This makes them one of the most promising targets for the upcoming huge interferometer experiments, being currently under construction in Europe (GEO600, VIRGO), Japan (TAMA) and the United States (LIGO). The expected rate of merging events is of the order of 10^{-5} per year per galaxy, estimated, with significant uncertainties, from population synthesis models and empirical data (see, e.g., Bulik, Belczynski, & Zbijewski 1999; Fryer, Woosley, & Hartmann 1999; Kalogera, & Lorimer 2000; and references therein). Templates are urgently needed to be able to extract the expected signals from background noise and to interpret the meaning of possible measurements.

Merging compact objects were suggested as possible sources of gamma-ray bursts (Blinnikov et al. 1984; Eichler et al. 1989; Paczyński 1991; Narayan, Piran, & Shemi 1991), but so far observations cannot provide convincing arguments for this hypothesis. In fact, the exciting detection of afterglows at other wavelengths of the electromagnetic spectrum by the Dutch-Italian *Bep-*

poSAX satellite and the discovery of lines in the afterglow spectra support the association of gamma-ray bursts (GRBs) with explosions of massive stars in star-forming regions of galaxies at high redshifts (e.g., Klose 2000, Lamb 2000). However, so far afterglows were discoverd only for GRBs with durations longer than a few seconds. Similar observations for the class of short, hard bursts ($\Delta t_{\rm GRB} \lesssim 2$ seconds; Mao, Narayan, & Piran 1994) are still missing, and we have neither a proof of their origin from cosmological distances, nor any hint on the astrophysical object they are produced by. NS+NS and NS+BH mergers are therefore still viable candidates for at least the subclass of short-duration bursts, in particular because such collisions of compact objects must occur at interesting rates, can release huge amounts of energy, and the energy is set free in a volume small enough to account for intensity fluctuations on a millisecond timescale. The ultimate proof of such an association would certainly be the coincidence of a GRB with a characteristic gravitational-wave signal.

Lattimer & Schramm (1974, 1976), Lattimer et al. (1977), and Meyer (1989) first considered merging neutron stars as a possible source of r-process nuclei. Their idea was that some matter might get unbound during the dynamical interaction. Since in neutron star matter neutrons are present with high densities and heavy nuclei can exist in surface-near layers, the environment might be suitable for the formation of neutron-rich, very massive nuclei. Detailed models are needed to answer the question how much matter can possibly be ejected during the merging, and what the nuclear composition of this material is.

Doing hydrodynamic simulations of the merging of compact stars is a challenging problem. Besides three-dimensional hydrodynamics, preferably including general relativity, the microphysics within the neutron stars is very complex. A nuclear equation of state (EoS) has to be used, neutrino physics may be important when the neutron stars heat up, magnetic fields might cause interesting effects, etc. Also high numerical resolution is required to account for the steep density gradient at the neutron star surface, and a large computational volume is needed if the ejection of matter is to be followed.

Different approximations and simplifications are possible when different aspects are in the main focus of interest. For example, the surface layers are unimportant and a simple ideal gas EoS $[P = (\gamma - 1)\varepsilon]$ and polytropic structure of the neutron stars can be used for parametric studies, when the gravitational-wave emission is to be calculated. This is an absolutely unacceptable simplification, however, when mass ejection and nucleosynthesis shall be investigated. For the latter problem as well as for the GRB topic, on the other hand, it is not clear whether general relativistic physics is essential. Nevertheless, of course, general relativity may be important to get quantitatively meaningful results. In particular, Newtonian models cannot answer the question whether and when a black hole is going to form after two neutron stars have merged.

Remarkable progress has been achieved during the past years. General relativistic simulations are in reach now, at least with simple input physics and for certain phases of the evolution of the binary systems, especially for the inspiraling phase (Duez, Baumgarte, & Shapiro 2000) and for the first stage of the final dynamical plunge (Shibata & Uryū 1999; Uryū, Shibata, & Eriguchi 2000), although the simulations become problematic once an apparent horizon begins to form. On the other hand, first attempts have been made to add

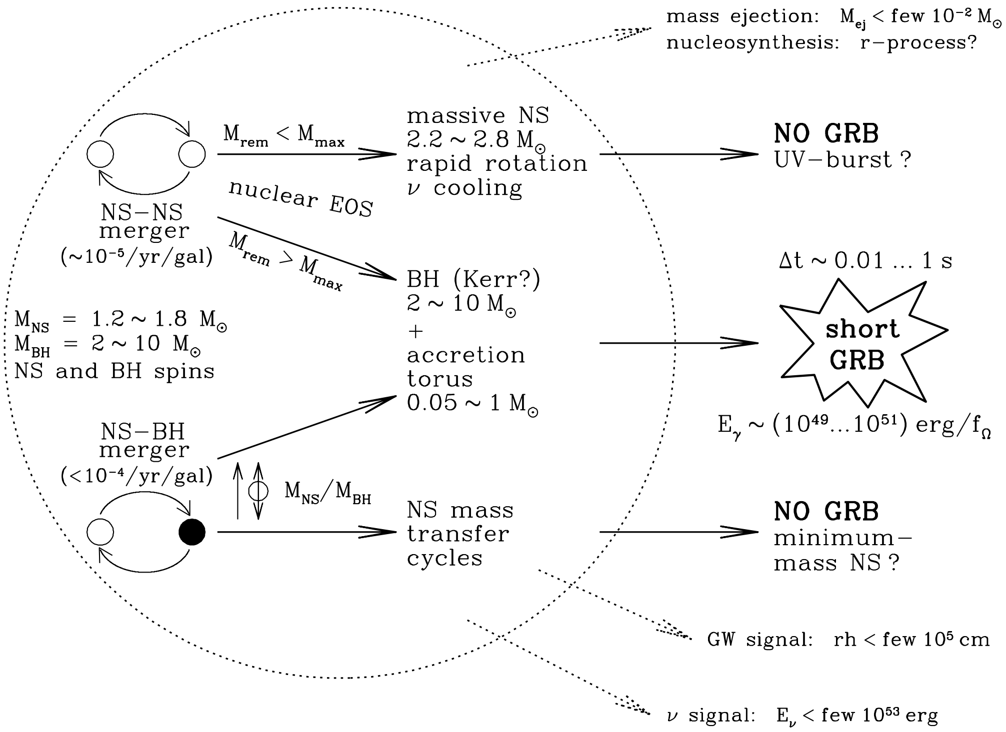

Figure 1. Possible evolution and observable signatures of NS+NS and BH+NS mergers. The evolution depends on the properties of the merging objects and the unknown conditions in the supranuclear interior of the neutron stars.

detailed microphysics, i.e., a physical nuclear EoS and neutrino processes, into Newtonian or to some degree post-Newtonian models (Ruffert, Janka, & Schäfer 1996; (Ruffert et al. 1997; Ruffert & Janka 1998, 1999; Rosswog et al. 1999, 2000). The hydrodynamics results were used in post-processing steps to draw conclusions on implications for GRB scenarios (Janka & Ruffert 1996, Ruffert & Janka 1999, Janka et al. 1999) and to evaluate the density-temperature trajectories of ejected matter for nucleosynthesis processes (Freiburghaus, Rosswog, & Thielemann 1999). The results, however, are not finally conclusive, because important effects have so far not been fully included and the simulations have to be improved concerning the resolution of the neutron star surfaces to reduce associated numerical artifacts.

2. Importance of the Nuclear Equation of State

Independent of numerical aspects and the unsatisfactory status of including general relativistic effects, one of the handicaps of merger models of compact stars are the unknown properties of the nuclear EoS. The compressibility of the nuclear EoS determines the neutron star structure and mass-radius relation. Therefore on the one hand, the evolution right before the merging, Roche-lobe overflow and the details of the final orbital instability and plunge of NS+NS binaries are affected by the neutron star EoS. On the other hand the possibility of episodic mass transfer and of cycles of orbital decay and widening in BH+NS systems depend on the EoS properties (Lattimer & Prakash 2000a; Lee & Kluźniak 1999a,b; Lee 2001). The nuclear EoS thus determines the dynamics and gravitational-wave emission during these phases. But also the post-merging evolution is very sensitive to the EoS properties. The NS+NS merger remnant can be a rapidly and differentially rotating, protoneutron-star like object. If the EoS is stiff, this object might not collapse to a black hole on a dynamical timescale, but its mass may be below the maximum stable mass of such a configuration. In this case the merger remnant might approach the final instability only on a much longer secular timescale, driven by neutrino emission, viscous and magnetic braking (Lipunova & Lipunov 1998) and angular momentum loss due to gravitational wave emission or mass shedding (Baumgarte & Shapiro 1998).

This could have very important implications for the gravitational-wave signal, because the emission might not be shut off immediately after the collision of the binary components, but — in particular in case of possibly developing triaxiality of the post-merger object — might continue for a considerable period of time. On the other hand, a hot, stable, massive protoneutron star-like object would cool by neutrino emission. Since neutrino energy deposition in the surface layers of the remnant causes a baryonic outflow of matter, similar to what happens in case of a protoneutron star at the center of a supernova, the merger site would be "polluted" by baryons and gamma-ray burst models might have a problem to explain the ejection of a baryon-poor pair-plasma fireball with highly relativistic velocities (Lorentz factors of several 100), which is needed to produce the visible gamma-ray emission. Of course, ways have been suggested to reduce or circumvent this problem, for example by considering a non-standard composition (strange quark matter) and structure (no baryonic crust, extreme compactness) of the merger remnant (e.g., Bombaci & Datta 2000; Mitra 2000; and references therein), or by invoking magnetic fields at the engine of the gamma-ray burst (e.g., Kluźniak & Ruderman 1998; Usov 1994).

The currently discussed EoSs for the supranuclear regime do not set strict limits for the maximum mass of neutron stars. Whereas the nuclear EoS around saturation density is expected to be rather stiff with a neutron star mass limit around 2 $M_\odot$ or larger, there is very little known about the EoS properties above twice nuclear matter density. A possible phase transition to a hyperonic state, kaon or pion condensates or a quark phase might soften the EoS and reduce the mass limit to significantly lower values (Lattimer & Prakash 2000b; Heiselberg & Pandharipande 2000; Balberg & Shapiro 2000; Weber 1999). Rigid rotation, on the other hand, can increase this limit by at most $\sim 20\%$, but differential rotation, which is likely to be present in the post-merger configuration, can stabilize compact stars with much larger masses (Baumgarte, Shapiro, & Shibata 2000). The degree of differential rotation in the remnant of a neutron star merger can only be determined by hydrodynamic simulations. On the other hand, the post-merging object is very massive (its baryonic mass is roughly twice the mass of a single neutron star), and due to the violence of the dynamical interaction of the merging stars the equilibrium density is overshot, thus favoring the gravitational collapse on a dynamical timescale even when an object with the combined mass of both neutron stars could find a stable rotational equilibrium.

Therefore firm theoretical predictions about the post-merging evolution of NS+NS systems are not possible at the moment, not even in case of a fully general relativistic treatment. Figure 1 summarizes possible evolutionary scenarios in dependence of the EoS properties and the masses and spins of the merging compact stars. When NS+NS and BH+NS merging leads to a (rapidly rotating) black hole surrounded by an accretion torus, energy can be released on the accretion timescale of the gas, which is 100 to 1000 times longer than the dynamical timescale of the system. In this case thermal energy of the hot, dense torus can be radiated through neutrinos, or rotational energy of the disk or black hole might be extracted by magnetic fields (Blandford & Znajek 1971; Li & Paczyński 2000). The efficiency of energy conversion to neutrinos or Poynting flux can be very high: A fair fraction of the rest mass energy of the accreted gas (up to several 10 per cent) or the rotational energy of the black hole can be released that way. Numerical values depend on the mass and the spin angular momentum of the black hole, on the strength of the magnetic fields and on the physical conditions in the accretion torus. Since the outflows occur preferentially along the rotational axis of the system, one hopes that the baryon loading problem can be avoided by the lower baryon densities above the poles of the black hole. Detailed models are necessary to make quantitative statements. Hydrodynamical simulations have been performed for the neutrino-powered scenario, although problems like the baryonic entrainment of the outflow and the lifetime of the accretion torus are still unanswered and require further refinement of the models. In case of the magnetohydrodynamic mechanism time-dependent simulations are extremely challenging and are currently not at the horizon.

Once bipolar outflow has formed, the question remains to be answered, what fraction of the kinetic or magnetic energy can finally be converted into gamma rays. Pessimistic estimates quote a few per cent or less, optimistic values claim several 10% (Kobayashi & Sari 2000).

Provided the remnant of a neutron star merger does not collapse to a black hole on a dynamical timescale, the baryon pollution problem is serious and probably hampers or destroys the chance for a gamma-ray burst. A massive, hot neutron star, which cools by neutrino emission, will poison its surroundings with a considerable amount of baryonic matter. Neutrino-driven winds might carry off $\sim 10^{-2}$ $M_\odot$ or more in all directions. This could have observable implications of such events, possibly generating a UV outburst of radiation when the expanding cloud dilutes to reach transparency (Li & Paczyński 1998). Concerning baryon pollution BH+NS mergers certainly offer an advantage because of the permanent presence of the black hole. The baryon pollution problem, however, might also occur there if the system runs into a state of long lasting, episodic mass transfer and the donating neutron star is not quickly disrupted into a disk. Circling around the black hole on a close orbit will lead to tidal heating of the neutron star and corresponding neutrino emission. In case of mass stripping of the neutron star down to its minimum mass, an explosion may occur, again possibly associated with the emission of radiation which is powered by radioactive decays in the expanding neutron star matter (Sumiyoshi et al. 1998).

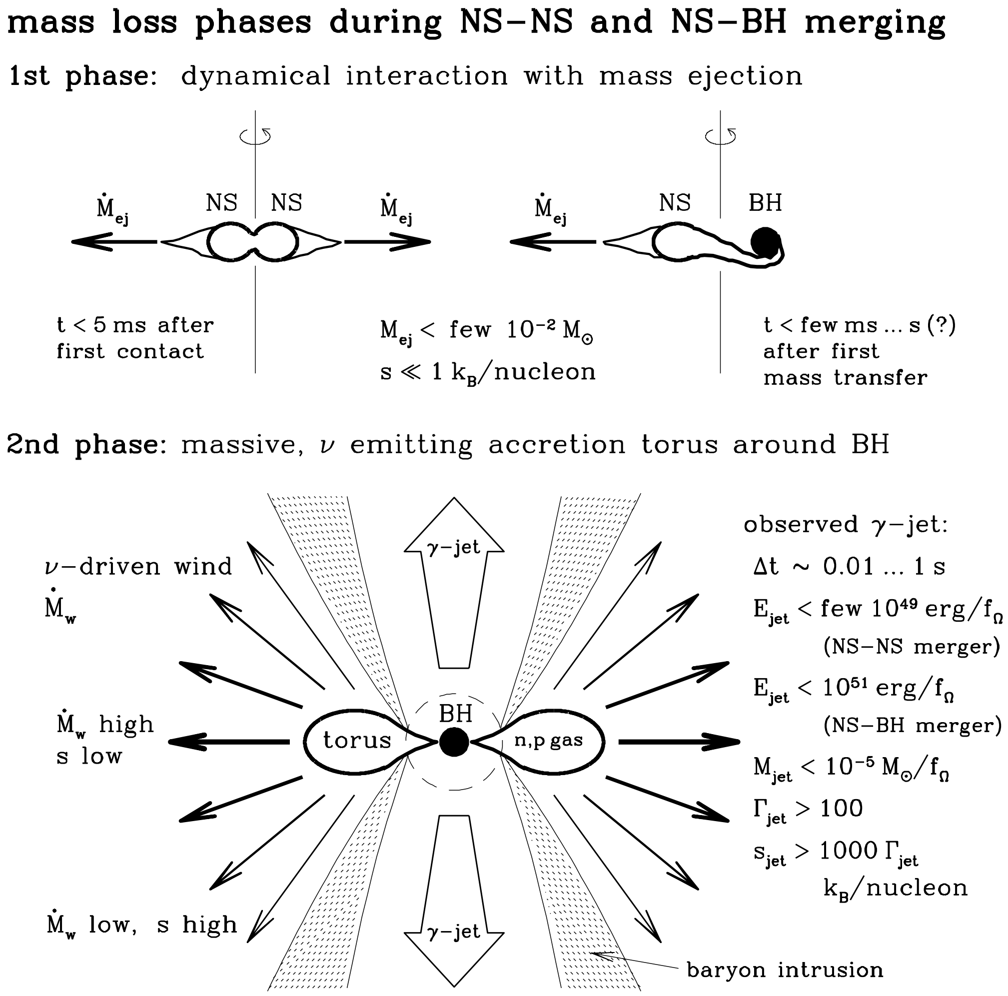

Figure 2. Phases of mass ejection from NS+NS and BH+NS mergers.

3. Nucleosynthesis in the Ejecta

Apart from a possible explosion of a neutron star at its minimum stable mass, two distinct processes can contribute to mass ejection from merger systems (Fig. 2). On the one hand, there is a phase of dynamical ejection of cold, low-entropy surface material of the merging neutron stars, which starts shortly after the two stars have fallen into each other and the neutron stars develop long tidal arms by centrifugal forces. The amount of mass loss depends very sensitively on the total angular momentum of the system and is largest when the neutron star spin(s) is (are) aligned with the orbital angular momentum vector. Decompressed neutron star surface matter expands and releases energy through radioactive decays or nucleon recombination to nuclei, which might help the flow to become gravitationally unbound. On the other hand, general relativity, if it leads to a quick collapse of the merger remnant to a black hole, might suppress the possibility of ejecting material from the tips of the tidal tails.

A second phase of mass loss is connected with the neutrino-driven wind. The matter will be neutrino-heated and hot, i.e., the entropies are very high. This plasma outflow is unavoidable when the neutron stars heat up and emit neutrinos, or when a hot, radiating accretion torus is swallowed by a black hole after the merging.

Nucleosynthesis calculations for the dynamically ejected matter of NS+NS mergers have been attempted (Freiburghaus et al. 1999), but the problem is not easy to attack. Not only the disregard of general relativity implies uncertainties, also the numerical resolution of the surface layers of the neutron stars has to be good enough to calculate the thermodynamical conditions precisely. The current models yield sufficiently large temperatures ($T \gtrsim 5 \times 10^9$ K) that the matter reaches nuclear statistical equilibrium (NSE) and the r-processing proceeds very similar to the classical r-process in the shock-heated, expanding matter of supernovae. With a suitable superposition of conditions (degree of neutronization for certain amounts of ejected matter) the integral abundance curve can be forced to fit the solar r-process abundance distribution. But what is the "actual" (model determined) neutronization of the ejecta? The effects of radioactive decays and neutrino production on the neutron density have to be taken into account to answer this question. And, also crucial, what are the "true" temperatures in the ejected gas? It is not certain that the gas in the very extended spiral arms ever reaches NSE temperature. If it stays cooler, the neutron-rich isotopes which are present in the outer layers of the neutron star, would be swept into the interstellar medium and after decaying, would reflect an abundance distribution different from the solar r-process pattern. In hydrodynamical models one has to fight against numerical viscosity when the temperature is to be calculated very accurately.

There is plenty of space for future work. Due to the lack of detailed models, nucleosynthesis has not been studied for the anisotropic neutrino-driven outflow of accreting black holes as merger remnants. In fact, the environment might provide suitable conditions of entropy and neutronization to obtain high-entropy r-processing. Such conditions can be verified in neutrino-driven winds of protoneutron stars in supernovae only in extreme corners of the parameter space for neutron star masses and radii (Qian & Woosley 1996; Otsuki et al. 2000; Sumiyoshi et al. 2000).

Table 1. NS+NS and BH+NS merger simulations

Model	Type	Masses $M_\odot$	Spin	$t_{\rm sim}$ ms	$t_{\rm ns}$ ms	$d_{\rm ns}$ km	$M_{\rm ns}^{\rm min}$ $M_\odot$	$\Delta M_{\rm ej}$ $M_\odot/100$
S64	NS+NS	1.2+1.2	solid	10	2.8	15	...	2.0
D64	NS+NS	1.2+1.8	solid	13	7.3	15	...	3.8
C64	NS+NS	1.6+1.6	anti	10	3.7	15	...	0.0085
A64	NS+NS	1.6+1.6	none	10	1.7	15	...	0.23
B64	NS+NS	1.6+1.6	solid	10	1.6	15	...	2.4
TN10	BH/AD	2.9+0.26	solid	15	...	...	...	...
C2.5	BH+NS	2.5+1.6	anti	10	2.6	11	0.78	0.01
A2.5	BH+NS	2.5+1.6	none	10	4.3	18	0.78	0.03
B2.5	BH+NS	2.5+1.6	solid	10	6.0	23	0.78	0.2
C5	BH+NS	5.0+1.6	anti	15	9.1	76	0.40	2.5
A5	BH+NS	5.0+1.6	none	20	16.3	65	0.52	2.5
B5	BH+NS	5.0+1.6	solid	15	10.8	79	0.50	5.6
C10	BH+NS	10.0+1.6	anti	10	8.0	96	0.65	2.2
A10	BH+NS	10.0+1.6	none	10	9.3	95	0.60	3.2
B10	BH+NS	10.0+1.6	solid	10	5.1	97	0.65	10.0

4. Computational Methods and Computed Models

Here we will only summarise the computational procedures that we used for doing NS+NS and BH+NS merger simulations. Details of the hydrodynamic method as well as the neutrino relevant algorithms can be found in Ruffert et al. (1996, 1997). The nested grid was described by Ruffert & Janka (1998) and Ruffert (1992). The implementation of the black hole was explained in Ruffert & Janka (1999), Eberl (1998) and Janka et al. (1999).

4.1. Methods

The hydrodynamical simulations were done with a code based on the Piecewise Parabolic Method (PPM) developed by Colella & Woodward (1984). The code is basically Newtonian, but contains the terms necessary to describe gravitational-wave emission and the corresponding back-reaction on the hydrodynamical flow (Blanchet et al 1990). The modifications that follow from the gravitational potential are implemented as source terms in the PPM algorithm, which are obtained from fast Fourier transforms. The necessary spatial derivatives are evaluated as standard centered differences on the grid.

In order to describe the thermodynamics of the neutron star matter, we use the EoS of Lattimer & Swesty (1991) for a compressibility modulus of bulk nuclear matter of $K = 180\,\mathrm{MeV}$ in tabular form. Use of a physical EoS instead of a simple ideal gas law implies that the adiabatic index is a function of space (i.e., of density, temperature and composition in the star) as well as of time (i.e., the value of the adiabatic index of the bulk of the matter changes when the neutron star strips some of its mass). This is an important difference compared to the polytropic neutron stars considered by Lee (2001). As mentioned above, the effective adiabatic index influences the dynamics of NS+NS and BH+NS mergers. An ideal gas description defines an idealized, "pure" condition, the "realistic" case is more complex.

Energy loss and changes of the electron abundance due to the emission of neutrinos and antineutrinos are taken into account by an elaborate "neutrino leakage scheme". The energy source terms contain the production of all types of neutrino pairs by thermal processes and additionally of electron neutrinos and antineutrinos by lepton captures onto baryons. The latter reactions act as sources or sinks of lepton number, too, and are included as source terms in a continuity equation for the electron lepton number. Matter is rendered optically thick to neutrinos due to the main opacity producing reactions, which are neutrino-nucleon scattering and absorption of electron-type neutrinos onto nucleons.

The presented simulations were done on multiply nested and refined grids. With an only modest increase in CPU time, the nested grids allow one to simulate a substantially larger computational volume while at the same time they permit a higher local spatial resolution of the merging stars. The former is important to follow the fate of matter that is flung out to distances far away from the merger site either to become unbound or to eventually fall back. The latter is necessary to adequately resolve the strong shock fronts and steep discontinuities of the plasma flow that develop during the collision. The procedures used here are based on the algorithms that can be found in Berger & Colella (1989), Berger (1987) and Berger & Oliger (1984). Each grid had 64^3 zones, the size of the smallest zone was $\Delta x = \Delta y = \Delta z = 0.64$ or $0.78\,\mathrm{km}$ in case of binary neutron stars and 1.25 or 1.5 km for BH+NS mergers. The zone sizes of the next coarser grid levels were doubled to cover a volume of 328 or 400 km side length for NS+NS and 640 or 768 km for BH+NS simulations.

In a post-processing step, performed after the hydrodynamical evolution had been calculated, we evaluated our models for neutrino-antineutrino ($\nu\bar{\nu}$) annihilation in the surroundings of the merged stars in order to construct maps showing the local energy deposition rates per unit volume. Spatial integration finally yields the total rate of energy deposition outside the neutrino emitting high-density regions.

4.2. Models and Initial Conditions

NS+NS merger simulations were started with two identical Newtonian neutron stars, or with neutron stars of different mass. In case of BH+NS coalescence we only considered neutron stars with a baryonic mass of about 1.63 $M_\odot$ so far, and varied the black hole mass. The distributions of density ρ and electron fraction $Y_e \equiv n_e/n_b$ (with n_e being the number density of electrons minus that of positrons, and n_b the baryon number density) were taken from a one-dimensional model of a cold, deleptonized (neutrino-less) neutron star in hydrostatic equilibrium and were the same as in Ruffert et al. (1996). The initial central temperature was set to a value of typically a few MeV, the temperature profile decreasing towards the surface such that the thermal energy was much smaller than the degeneracy energy of the matter.

For numerical reasons the surroundings of the neutron stars cannot be treated as completely evacuated. The density of the ambient medium was set to less than 10^8 g/cm^3, more than six orders of magnitude smaller than the central densities of the stars. The total mass on the whole grid, associated with this finite background density is less than $10^{-3}\, M_\odot$.

We prescribed the orbital velocities of the coalescing neutron stars according to the motions of point masses, as computed from the quadrupole formula. The tangential components of the velocities of the neutron star centers correspond to Kepler velocities on circular orbits, while the radial velocity components reflect the emission of gravitational waves leading to the inspiral of the orbiting bodies.

A spin of the neutron stars around their respective centers was added to the orbital motion and was varied from model to model: The "A" models do not have any additional spins added on top of their orbital velocity. In this case all parts of the neutron stars start out with the same absolute value of the velocity, also called 'irrotational' motion. The angular velocity (both magnitude and direction) of the spin in "B" models is equal to the angular velocity of the orbit. This results in a 'solid body' type (tidally locked) motion, also called 'corotating'. "C" models represent counter-rotating cases where spins and orbital angular momentum vectors have opposite directions.

We do not relax the neutron stars to equilibrium states before we start the simulations. Instead, we set the initial distances to sufficiently large values that most of the induced oscillations have been damped away by numerical viscosity before the dynamical phase of the merging is reached. Test calculations with even larger distances do not exhibit significant differences of the evolution. We are therefore pretty confident that the final orbital instability due to the finite size of the objects was not affected by the non-equilibrated initial state.

Table 1 gives a list of computed NS+NS and BH+NS merger models, for which the physical parameters of the systems were varied ($t_{\rm sim}$ is the time interval covered by the simulation, $t_{\rm ns}$ the time when the two density maxima of the neutron stars are a stellar radius, i.e., $d_{\rm ns} = 15\,$km, apart, and $\Delta M_{\rm ej}$ the amount of dynamically ejected matter). Besides the baryonic mass of the neutron star(s) and the mass of the black hole, the spins of the neutron stars were varied. "Solid" means synchronously rotating stars, "none" irrotational cases, and "anti" counter-rotation, i.e., spin angular momenta opposite to the direction of the orbital angular momentum vector. In addition to the listed models, we performed simulations where we changed numerical aspects, for example the resolution, initial distances and initial temperatures, or used an entropy equation to follow the temperature evolution. In particular, the stability of the numerical handling, the smallness of the effects due to numerical viscosity and finite resolution, and the quality of energy and angular momentum conservation were confirmed by BH+NS runs, where we followed the decay of the orbit for a large number (~ 10) of full revolutions.

The cool neutron stars with baryonic masses of 1.2, 1.63 or 1.8$\,$M$_\odot$ have a radius around 15$\,$km (Ruffert et al. 1996), the radius increasing weakly with the stellar mass. The runs in Table 1 were started with a center-to-center distance of 42–46$\,$km for NS+NS and with 47$\,$km in case of BH+NS for $M_{\rm BH} = 2.5\,{\rm M}_\odot$, 57$\,$km for $M_{\rm BH} = 5\,{\rm M}_\odot$ and 72$\,$km for $M_{\rm BH} = 10\,{\rm M}_\odot$. The simulations were stopped at a time $t_{\rm sim}$ between 10$\,$ms and 20$\,$ms. The black hole was treated as a point mass at the center of a sphere with radius $R_{\rm s} = 2GM_{\rm BH}/c^2$ which gas could enter unhindered. Its mass and momentum were updated along with the accretion of matter.

Model TN10, which is added for comparison, is a continuation of the NS+NS merger Model B64, where at time $t = 10\,\mathrm{ms}$ the formation of a black hole with a mass of $2.5\,\mathrm{M}_\odot$ was assumed, and the accretion of the remaining gas on the grid ($\sim 0.7\,\mathrm{M}_\odot$) was followed for another 5 ms until a quasi-steady state was reached. Different times for the black hole collapse were tested ($\sim$ 1, 2, 3 and 9 ms after the neutron stars had merged to one body), and gave qualitatively similar results (Ruffert & Janka 1999).

5. Results

In this proceedings contribution the results of our models can only be outlined. The results pertaining to the accretion of a high-density torus by a black hole can be found in Ruffert & Janka (1999). Latest models for neutron star merger simulations (the ones discussed here) will be published fully in Ruffert & Janka (2001, in preparation), older calculations (obtained with a less complete version of our code) were published by Ruffert et al. 1996, 1997), while the BH+NS simulations are summarized in Janka et al. (1999) and were reported in detail by Eberl (1998).

5.1. Dynamical Evolution and Mass Ejection

Figure 3 shows the temporal evolution of the density distribution in the orbital plane for both Models A64 and B64. Initially, the orbits of the two neutron stars decay due to gravitational radiation, and the stars approach each other slowly. Once the distance decreases below the instability limit, the final plunge occurs (upper panels). Note that Model B64, which has more total angular momentum, develops prominent spiral arms in which matter is flung out to large distances (right middle panel) and a considerable amount of matter carries enough mechanical energy to escape the system ($\Delta M_{\mathrm{ej}} \sim 2 \times 10^{-2}\,\mathrm{M}_\odot$, see Table 1). Model A64, on the contrary, remains more compact during this very early post-merging phase (left middle panel). The amount of ejected mass for the A-model is therefore about one order of magnitude lower. After 10 ms a very dense, nearly spherical central object has formed, surrounded by a less dense, extended, thick equatorial torus. When a steady state has been reached, the densities in this cloud are rather similar in both simulations (lower panels).

With a Newtonian code we cannot determine whether and if, when, the merger remnant collapses to a black hole. In order to investigate what happens in such a case, we continued Run B64, assuming that such a catastrophe happens to the central, dense body on a dynamical timescale of a few milliseconds after the merger. In the simulation listed in Table 1 (Model TN10) this gravitational instability was assumed to occur at the end of the computed merger evolution at $t = 10\,\mathrm{ms}$. A Newtonian potential,

$$\Phi_{\mathrm{N}} = -\frac{GM_{\mathrm{BH}}}{r} , \tag{1}$$

was taken for the black hole. In order to include the effects associated with the existence of an innermost stable circular orbit at a radius of $3R_{\mathrm{s}} = 6GM_{\mathrm{BH}}/c^2$,

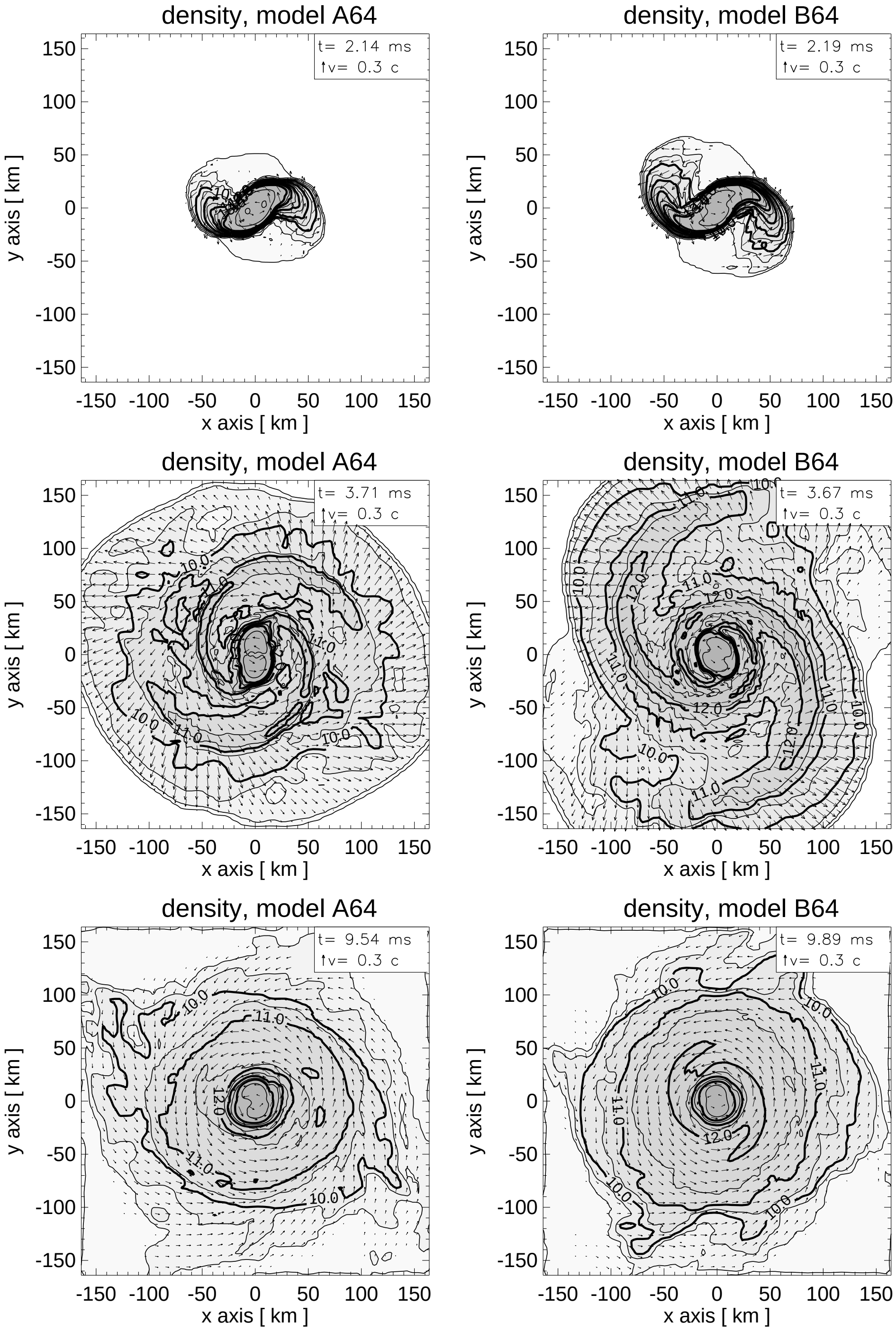

Figure 3. Density contours in the orbital plane for the NS+NS merger Models A64 (left column) and B64 (right column). The density (in g/cm^3) is shown logarithmically, the contours being spaced with intervals of 0.5 dex. The arrows indicate the velocity field. The time is given in the upper right corner of the plots.

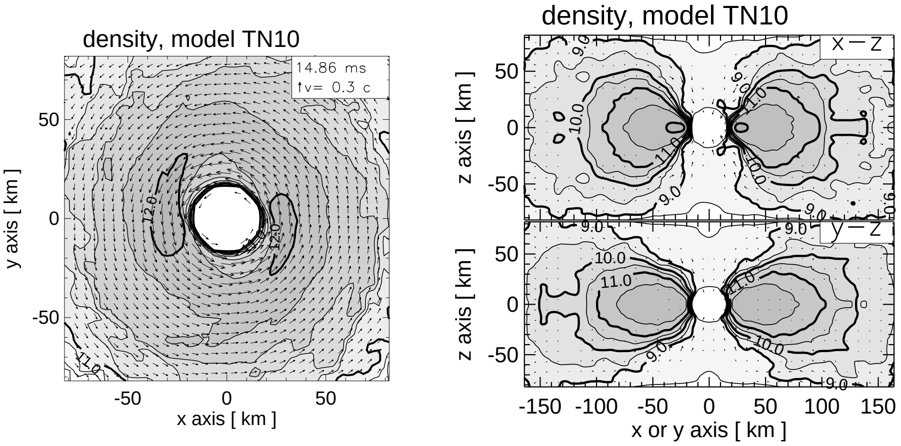

Figure 4. Contour plots of the Newtonian Model TN10 in the equatorial plane (left) and perpendicular to it (right) near the end of the simulation. The density is displayed together with the velocity field. The density is measured in g cm^{-3} and its contours are spaced logarithmically with intervals of 0.5 dex. The time elapsed from the beginning of the simulation is about 15 ms.

we compared these results with a second (set of) simulation(s), in which the gravitational potential was described by the pseudo-Newtonian expression,

$$\Phi_{\mathrm{PW}} \equiv -\frac{GM_{\mathrm{BH}}}{r - R_{\mathrm{s}}} \tag{2}$$

(Paczyński & Wiita 1980).

The black hole at the center of the computational grid was represented by a vacuum sphere with a radius of $2R_{\mathrm{s}}$ instead of $1R_{\mathrm{s}}$ as in the BH+NS merger simulations. The gain of mass, momentum, angular momentum and energy by the black hole due to the accretion of gas were also monitored during the simulations. In the grid zones that were located inside the vacuum sphere (these zones were not removed from the hydrodynamic grid), the mass density was continuously reset to a negligibly small but finite value of $10^8\,\mathrm{g\,cm^{-3}}$, and a correspondingly very small value of the pressure was present.

After $\sim$ 5 ms of simulated accretion Model TN10 has reached a quasi-stationary state where the black hole has a mass of $2.9\,\mathrm{M}_\odot$ and the accretion torus contains $M_{\mathrm{d}} \sim 0.26\,\mathrm{M}_\odot$ of gas. The density structure at this time is shown in Fig. 4. The left plot gives the density in the equatorial plane, the right one shows it in the x-z- and y-z-planes perpendicular to the equatorial plane. The contour for density $\rho = 10^{10}\,\mathrm{g\,cm^{-3}}$ extends out to a radius of 120 km, and the average density of the torus is about $3\times10^{11}\,\mathrm{g\,cm^{-3}}$. At the end of the simulation the torus has become nearly axially symmetric with only minor deviations. The accretion rate by the black hole ist $\dot{M} \sim 5\ \mathrm{M}_\odot\,\mathrm{s}^{-1}$, which allows one to estimate the duration of this accretion phase to $t \sim 53\,\mathrm{ms}$. The evolution is driven by angular momentum transport/loss due to numerical viscosity, corresponding to an effective α-viscosity of $\alpha_{\mathrm{eff}} \sim 4 \times 10^{-3}$ (Table 2 and Ruffert & Janka 1999).

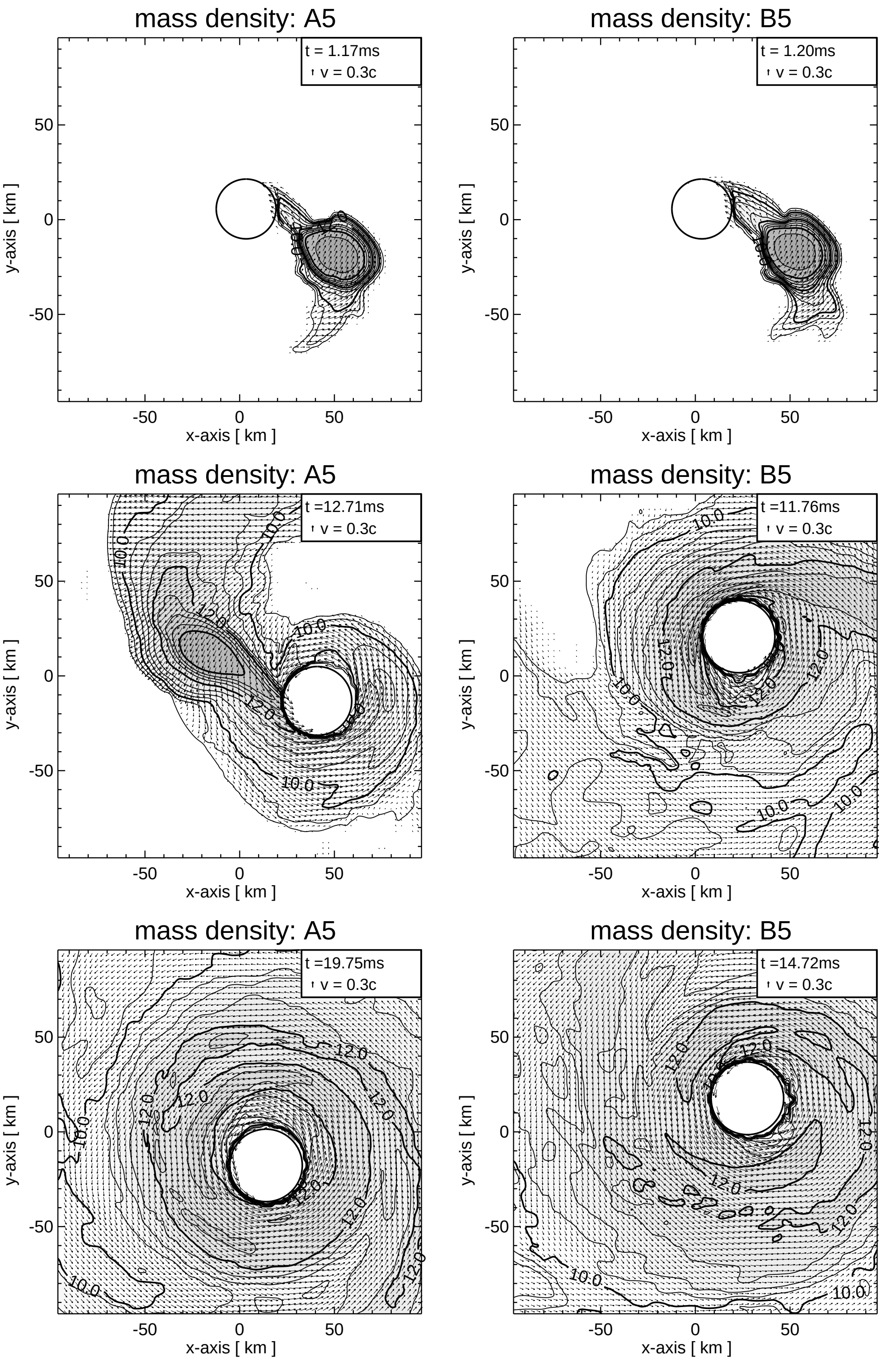

Figure 5. Density contours in the orbital plane for the BH+NS merger Models A5 (left column) and B5 (right column). The density (in g/cm^3) is shown logarithmically, the contours being spaced with intervals of 0.5 dex. The arrows indicate the velocity field. The time is given in the upper right corner of the plots.

Table 2. Accretion phase and neutrino annihilation

Model	$M_{\rm d}$ $M_\odot$	$\dot{M}_{\rm d}$ $M_\odot/{\rm s}$	$t_{\rm acc}$ ms	$\alpha_{\rm eff}$ 10^{-3}	$a_{\rm i}$	$a_{\rm f}$	$a_{\rm BH}^{\infty}$	$\langle L_\nu\rangle$ $100\,\frac{\rm foe}{\rm s}$[a]	$\dot{E}_{\nu\bar\nu}$ foe/s	q_ν %	$q_{\nu\bar\nu}$ %	E_ν foe	$E_{\nu\bar\nu}$ foe
S64	...	...	...	...	0.98	0.75	...	1.5	1	...	1	...	...
D64	...	...	...	...	0.87	0.69	...	2	2	...	1	...	...
C64	...	...	...	...	0.64	0.49	...	4	9	...	2	...	...
A64	...	...	...	...	0.76	0.55	...	5	9	...	2	...	...
B64	...	...	...	...	0.88	0.63	...	3	7	...	2	...	...
TN10	0.26	5	53	4	...	0.42	0.59	1.2	0.5	1.3	0.4	7	0.03
C2.5	0.26	6	43	4	0.65	0.47	0.60	7	20	6	3	30	0.9
A2.5	0.33	<14	>24	<8	0.67	0.39	0.56	7	20	>3	3	>17	>0.5
B2.5	0.45	<35	>13	<14	0.69	0.38	0.61	7	20	>1	3	>9	>0.3
C5	0.38	5	76	5	0.44	0.27	0.42	4	8	4	2	30	0.6
A5	0.49	6	82	4	0.45	0.17	0.37	4	8	4	2	33	0.7
B5	0.45	6	75	5	0.46	0.19	0.38	4	8	4	2	30	0.6
C10	0.67	<10	>67	<11	0.24	0.07	0.25	2	2	>1	1	>13	>0.1
A10	0.56	<60	>9	<82	0.25	0.07	0.22	2	2	>0.2	1	>2	>0.02
B10	0.47	3	160	5	0.25	0.11	0.23	2	2	4	1	32	0.3

[a] 1 foe = 10^{51} erg (**f**ifty **o**ne **e**rg).

Near the poles of the black hole and along the system axis, the density has decreased to values below $5\times10^8\,{\rm g\,cm^{-3}}$. This is only one order of magnitude above the lower density limit which was set to $5\times10^7\,{\rm g\,cm^{-3}}$ in the surroundings of the torus for numerical reasons, but nevertheless it is about 3 orders of magnitude below the average density inside the torus. In this sense we see the cleaning of the region along the rotational axis of the black hole-torus system into of an "evacuated", cylindrical funnel with opening half-angle of roughly 50 degrees. Material which was swept into the polar regions during and immediately after the merging of the neutron stars falls into the newly formed black hole very quickly within a free-fall timescale, because it is not supported by centrifugal forces. This offers favorable conditions for the formation of a baryon-poor, jetted outflow, powered by neutrino-antineutrino annihilation.

The evolution of the density distributions of the BH+NS merger Models A5 and B5 is shown in Fig. 5. During its first approach, Roche lobe overflow occurs (upper panels) and the neutron star transfers matter to the black hole at huge rates of several 100 up to $\sim 1000\,{\rm M_\odot\,s^{-1}}$. Within 2–3 ms it loses 50–75% of its initial mass. In case of the $2.5\,{\rm M_\odot}$ black hole the evolution is catastrophic and the neutron star is immediately disrupted (for details, see Janka et al. 1999). A mass of 0.2–0.3 $M_\odot$ remains in a thick disk around the black hole ($M_{\rm d}$ in Table 2). In contrast, the neutron star survives and is kicked on an elliptical orbit for $M_{\rm BH} = 5\,{\rm M_\odot}$ and $10\,{\rm M_\odot}$, In this case the orbital distance increases again and a significantly less massive neutron star begins a second approach. Near the periastron passage, the black hole again swallows gas at rates of more than $100\,M_\odot/{\rm s}$. Even a third episode of mass transfer is possible (middle panels). Finally, at a distance $d_{\rm ns}$ and time $t_{\rm ns}$ the neutron star with a mass of $M_{\rm ns}^{\rm min}$ is destroyed (Table 1) and most of its mass ends up in an accretion torus (Table 2, lower panels of Fig. 5).

The mass tranfer is not stable Roche lobe overflow, but occurs in a catastrophic, episodic way. After at most a few approaches, the neutron star is finally torn apart by gravitational forces. Note that in case of a physical equation of state, different from the ideal gas case, the neutron star mass is bounded by a lower limit. Below this limit the effective adiabatic index becomes smaller than 4/3 and a stable configuation is not possible. In case of cold neutron stars, the lower mass limit is typically around 0.1–$0.2\,\mathrm{M}_\odot$. If the neutron stars are hot (dimensionless entropies between 1 and 2 per nucleon, corresponding to temperatures up to a few 10 MeV) and/or lepton-rich, this lower mass limit can be as large as 0.8–$1\,\mathrm{M}_\odot$ (see, e.g., Gondek, Haensel, & Zdunik 2000). Although in our simulations the temperatures do not become that high because there is only little heating, the neutron star masses at the moment of destruction are near this value. The reason for this is the tidal stretching of the stars, which reduces their central densities below the critical density where the adiabatic index drops to values smaller than 4/3. This destabilizes the neutron stars and leads to their final disruption. Therefore a realistic equation of state does not allow a large number of mass transfer cycles.

During the merging of BH+NS systems a gas mass ΔM_{ej} between $\sim 10^{-4}\,M_\odot$ in case of counter-rotation and $M_{\mathrm{BH}} = 2.5\,M_\odot$, and $\sim 0.1\,M_\odot$ for corotation and $M_{\mathrm{BH}} = 10\,M_\odot$ is dynamically ejected (Table 1). In the latter case the associated angular momentum loss is about 7%, in all other cases it is less than 5% of the total initial angular momentum of the system. Another fraction of up to 24% of the initial angular momentum is carried away by gravitational waves. In Table 2 the rotation parameter $a = Jc/(GM^2)$ is given for the initial state of the binary system (a_{i}) and at the end of the simulation (a_{f}) for the remnant of NS+NS mergers or for the black hole in BH+NS systems, respectively, provided the black hole did not have any initial spin. When the whole disk mass M_{d} has been swallowed by the black hole, which is spun up, a final value a_{BH}^{∞} can be estimated by assuming accretion of a corotating, thin disk with maximum radiation efficiency (Table 2).

At the end of the simulations, several of the BH+NS models have reached a steady state, characterized by only a "slow" growth of the black hole mass with a nearly constant accretion rate. Corresponding rates $\dot{M}_{\mathrm{d}}$ are given in Table 2 and are several $M_\odot$ per second. With typical torus masses M_{d} of several tenths of a solar mass, we estimate torus life times $t_{\mathrm{acc}} = M_{\mathrm{d}}/\dot{M}_{\mathrm{d}}$ of 50–150 ms. Values with $>$ and $<$ signs indicate cases where the evolution and emission are still strongly time-dependent at the end of the computation. In these cases the accretion torus around the black hole has also not yet developed axial symmetry. In all other cases the further disk evolution is mainly driven by the angular momentum transport mediated by viscous shear forces, which determine the accretion rate. In the simulations the viscosity is associated with the finite chosen resolution of the hydro code (which solves the Euler equations), instead of a physical mechanism which creates viscosity. The corresponding α parameter can be estimated to be $\alpha_{\mathrm{eff}} \sim 5\times 10^{-3}$ (Table 2), not an unrealistic value for accretion disks.

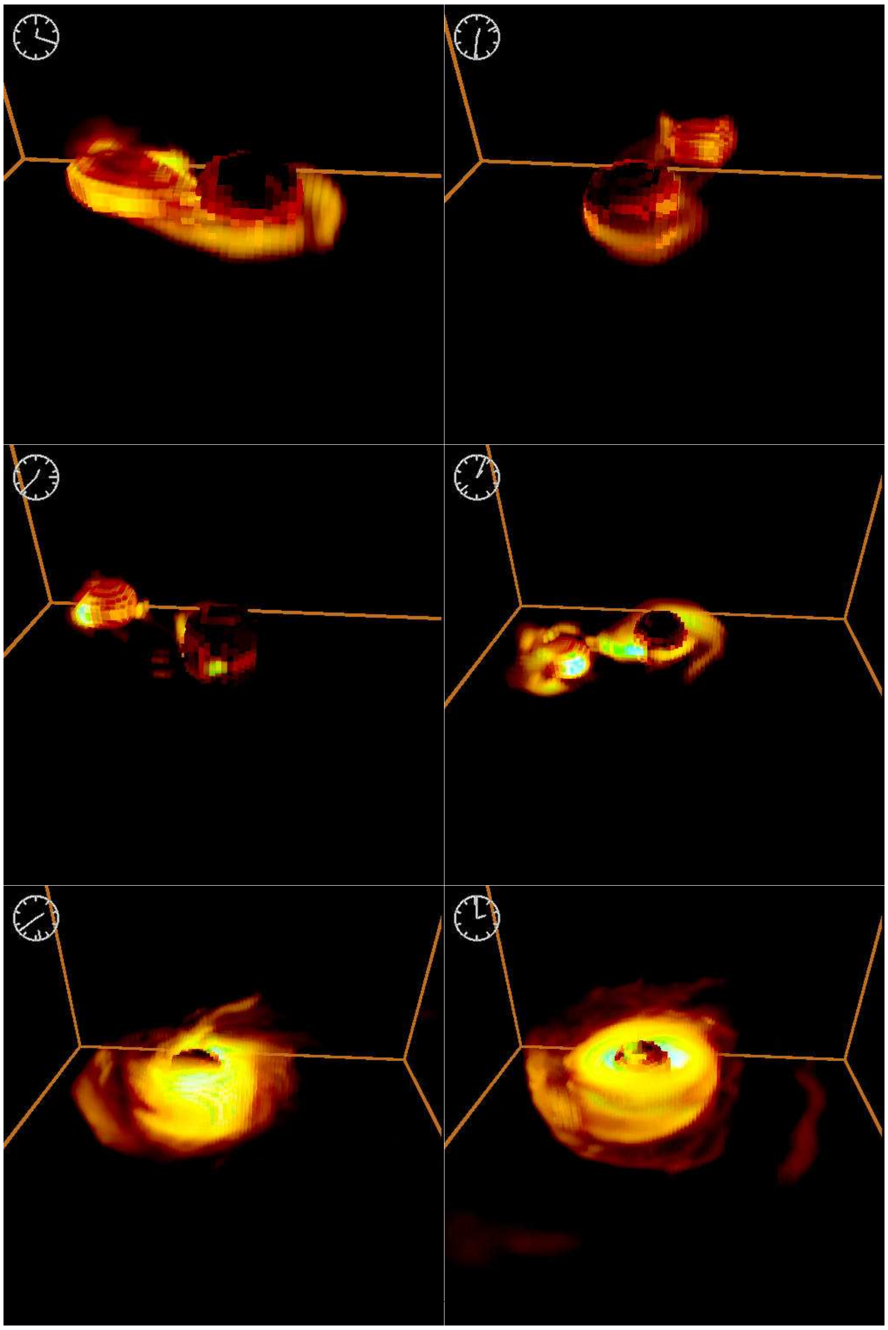

Figure 6. Ray-tracing images of six stages during the merging of a neutron star with a $5\,M_\odot$ black hole (Model A5). The corresponding times from top left to bottom right are 3.0 ms, 5.2 ms, 6.3 ms, 10.7 ms, 16.5 ms and 20.0 ms after the start of the simulation. The images visualize the neutrino emission. Bright regions are dense and emit neutrinos from optically thick conditions.

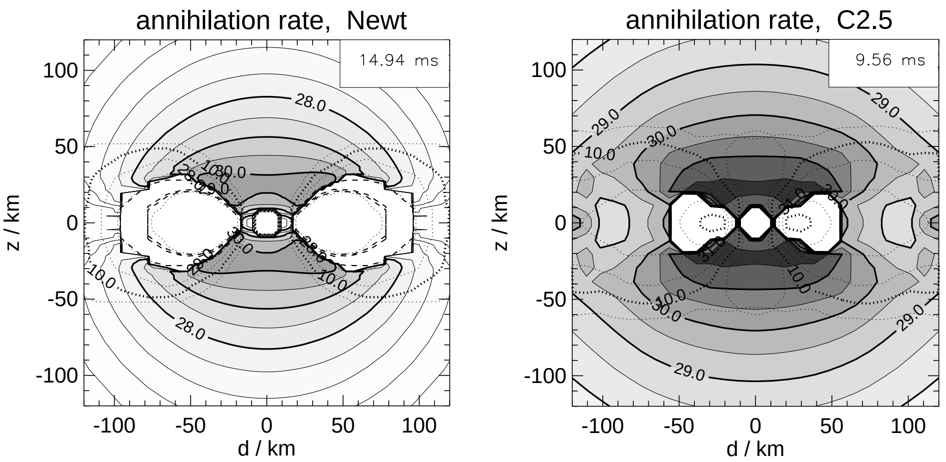

Figure 7. Energy deposition in the vicinity of a black hole by the annihilation of neutrino-antineutrino pairs emitted from a hot accretion torus. The left plot shows the situation after the NS+NS merging in Model TN10, the right figure is the result of the BH+NS merger Model C2.5. The white circles at the center represent the black hole, the solid contours give the azimuthally averaged energy deposition rate per unit volume (erg per cm^3 per s) and the dashed contours show the density distribution of the tori.

5.2. Neutrino Emission and Gamma-Ray Bursts

Compressional heating, shear due to numerical viscosity, and dissipation in shocks heat the gas in the merging neutron stars and in the accretion flow to the black hole. After a few milliseconds the maximum temperatures in the NS+NS merger remnant have climbed to several 10 MeV (Table 3). This is also the typical timescale until the thermodynamic conditions in the accretion torus around the black hole reach a steady state with average temperatures around 10 MeV and densities between $10^{10}\,\mathrm{g/cm^3}$ and $10^{12}\,\mathrm{g/cm^3}$. At such conditions electron and positron pairs are abundant, and electron neutrinos and antineutrinos are copiously produced by $e^{\pm}$ capture reactions on free nucleons

$$p + e^- \longrightarrow n + \nu_e \quad \text{and} \quad n + e^+ \to p + \bar{\nu}_e \ . \tag{3}$$

Muon and tau neutrino and antineutrino pairs are also emitted by e^+e^- annihilation but contribute to the energy loss at a minor level. The accretion flow is not transparent to neutrinos and effects due to their finite diffusion time have to be taken into account when the neutrino luminosity is calculated. In Fig. 6 the thermal evolution of the BH+NS merger Model A5 can be seen from ray-tracing images which visualize the neutrino emission.

Table 3 provides information about the maximum and time-averaged luminosities ($L_{\nu_i}^{\max}$ and $L_{\nu_i}^{\mathrm{av}}$, respectively) for ν_e and $\bar{\nu}_e$ and for the sum of all heavy-lepton neutrinos (which are denoted by $\nu_x \equiv \nu_\mu, \bar{\nu}_\mu, \nu_\tau, \bar{\nu}_\tau$). The total neutrino emission fluctuates strongly in response to dynamical processes, in particular rises dramatically during mass transfer episodes in BH+NS mergers. In case of NS+NS mergers there is a more monotonic increase with time. The average energies of emitted neutrinos, $\langle\epsilon_\nu\rangle$, are typically about 15 MeV for electron

Table 3. Gravitational waves and neutrinos

Model	$L_{\rm GW}^{\rm max}$	$rh^{\rm max}$	$E_{\rm GW}$	$L_{\nu_e}^{\rm max(av)}$	$L_{\bar\nu_e}^{\rm max(av)}$	$L_{\Sigma\nu_x}^{\rm max(av)}$	E_ν	$kT^{\rm max}$	$\langle\epsilon_{\nu_e}\rangle$	$\langle\epsilon_{\bar\nu_e}\rangle$	$\langle\epsilon_{\nu_x}\rangle$
	$10^4\,\frac{\rm foe}{\rm s}$ [a]	10^4cm	foe	$100\,\frac{\rm foe}{\rm s}$	$100\,\frac{\rm foe}{\rm s}$	$100\,\frac{\rm foe}{\rm s}$	foe	MeV	MeV	MeV	MeV
S64	0.7	5.5	14	0.3(0.2)	0.9(0.5)	0.3(0.2)	0.8	35	12	18	26
D64	0.4	5.5	13	0.5(0.3)	1.3(0.8)	0.7(0.4)	1.1	35	13	19	27
C64	1.2	6.0	23	1.1(0.5)	2.6(1.3)	0.7(0.3)	1.9	69	13	19	27
A64	2.1	8.6	52	0.9(0.5)	2.6(1.3)	1.4(0.6)	2.3	39	12	18	26
B64	2.1	8.9	37	0.6(0.4)	1.8(1.1)	0.9(0.4)	1.8	39	13	19	27
TN10	...	...	...	0.5(0.4)	1.3(0.9)	0.6(0.2)	0.8	15	9	13	21
C2.5	2.3	9.9	32	1.5(0.5)	7.3(2.5)	5.2(1.9)	4.5	74	16	22	31
A2.5	2.0	9.9	50	1.8(0.5)	6.4(2.2)	3.1(1.3)	3.6	65	15	22	31
B2.5	2.1	9.6	61	0.9(0.3)	6.5(1.7)	3.6(0.9)	2.5	61	14	21	29
C5	3.9	13.0	50	0.7(0.4)	3.8(1.6)	2.5(1.1)	4.5	46	15	20	29
A5	3.2	14.8	102	0.7(0.2)	4.4(1.5)	2.8(0.8)	4.5	51	16	24	31
B5	3.4	14.5	95	0.6(0.2)	3.7(1.1)	2.5(0.6)	2.9	44	14	21	28
C10	7.1	21.9	123	0.4(0.1)	2.5(0.4)	1.2(0.1)	0.6	51	14	19	24
A10	6.9	26.2	168	0.2(0.1)	2.5(0.5)	1.2(0.2)	0.7	50	14	20	26
B10	7.3	26.2	163	0.4(0.1)	2.5(0.8)	1.4(0.2)	1.1	52	13	18	24

[a] 1 foe = 10^{51} erg (**f**ifty **o**ne **e**rg).

neutrinos, about 20 MeV for electron antineutrinos and about 30 MeV for muon and tau neutrinos and antineutrinos. The total energy E_ν radiated in neutrinos within the computed 10–20 ms of the evolution is a few 10^{51} erg. In case of BH+NS mergers, in particular for smaller black holes, the neutrino luminosities and mean energies are significantly higher than for NS+NS mergers.

The black hole continues to swallow matter from the accretion torus for a period between several ten milliseconds and possibly a fair fraction of a second (Table 2). During this time the hot gas will continue to radiate neutrinos. We cannot follow this long-time evolution by hydrodynamical models, but attempt to derive rough estimates by extrapolating the conditions present at the end of our simulations. With average total neutrino luminosities $\langle L_\nu\rangle$ of several 10^{53} erg s^{-1} the accretion tori lose a total energy of a few 10^{52} erg in neutrinos (E_ν in Table 2), which equals up to 4–6% of the rest-mass energy of the accreted matter [$q_\nu \equiv E_\nu/(M_{\rm d}c^2)$]. Because the BH-torus configuration is very compact and neutrinos are emitted at very high luminosities, the annihilation of neutrino-antineutrino pairs, $\nu\bar\nu \to e^+e^-$, in the vicinity of the black hole is rather efficient, depositing an energy $E_{\nu\bar\nu}$ of nearly 10^{51} erg (Table 2) in a pair-plasma cloud above the poles of the black hole (Fig. 7). Peak rates of this energy deposition exceed 10^{52} erg/s. The efficiency of energy conversion from neutrinos to $e^\pm$ pairs, $q_{\nu\bar\nu} \equiv E_{\nu\bar\nu}/E_\nu$, is of the order of 1–3 per cent (Table 2).

5.3. Gravitational-Wave Emission

While the neutrino emission rises gradually after the final plunge of binary neutron stars, the gravitational-wave emission peaks at the moment of the collision of the stars. In case of BH+NS mergers the maximum gravitational-wave lumi-

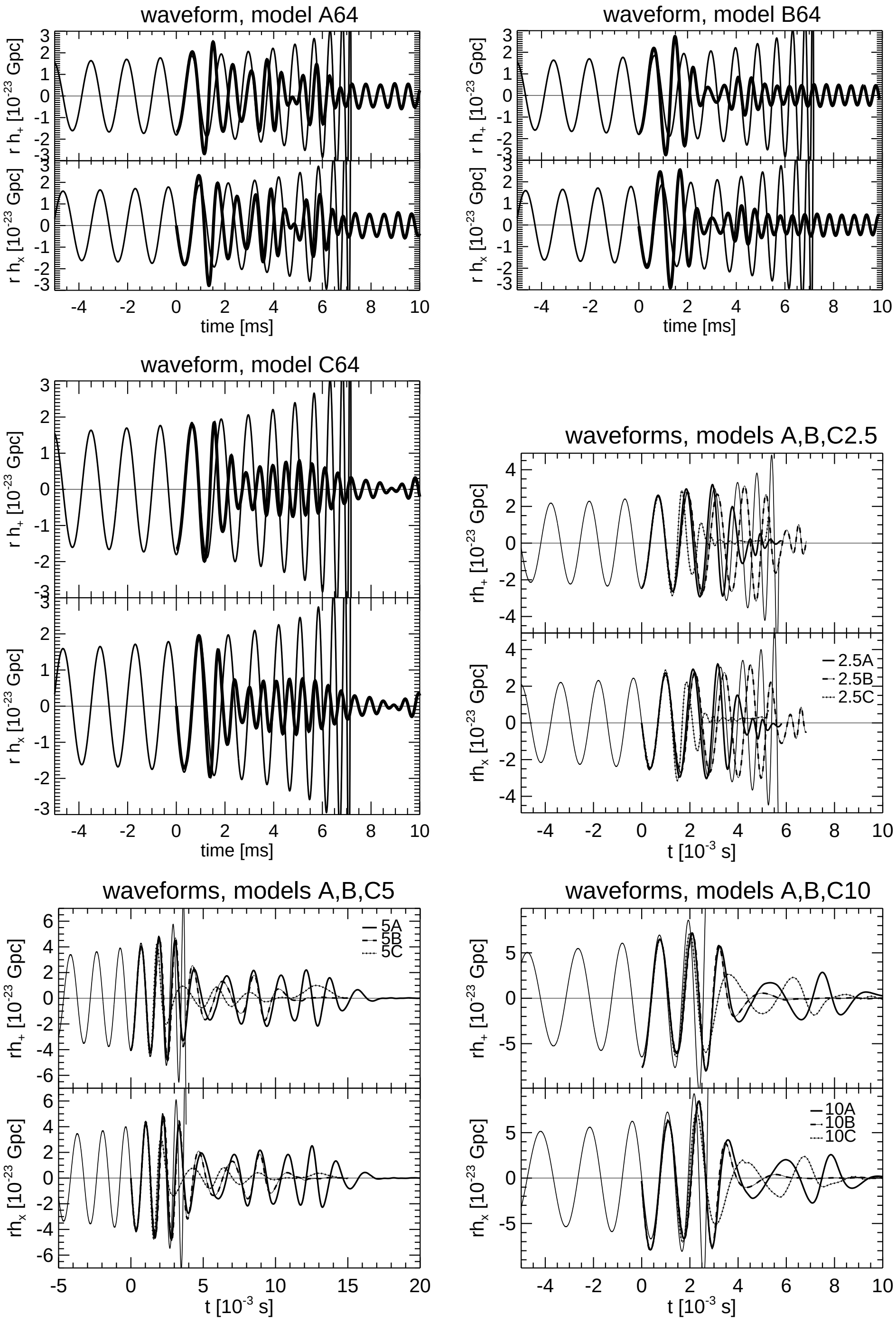

Figure 8. Gravitational waveforms for NS+NS merger Models A64, B64 and C64 and all BH+NS merger models listed in Table 1. Time is measured in ms from the start of the simulation, the observer is located perpendicular to the orbital plane. The thin solid lines correspond to the chirp signal of two point masses.

nosity coincides with the phase when the mass transfer rate to the black hole is largest, which occurs during the first approach of the neutron star (between 2 and 5 ms after the start of the simulations). Afterwards the neutron star is either disrupted to an essentially axi-symmetric accretion torus (in case of a $2.5\,\mathrm{M}_\odot$ black hole) or has been stripped to a significantly less massive body. Both reduces the production of gravitational waves. The maximum gravitational-wave luminosity $L_{\rm GW}^{\rm max}$ and the wave amplitude rh (for distance r from the source) increase with the black hole mass and with the masses of the merging neutron stars (Table 3). $L_{\rm GW}^{\rm max}$ can reach values of nearly 10^{56} erg s^{-1} in case of $10\,\mathrm{M}_\odot$ black holes, and the total energy radiated in gravitational waves, $E_{\rm GW}$, can be as high as $0.1\,\mathrm{M}_\odot c^2$. Fourier spectra of the emitted waves peak between 800 and 1000 Hz, with the dominant frequency of the emission decreasing with the black hole mass.

Figure 8 shows typical waveforms for NS+NS and BH+NS mergers. The numerical simulations reproduce the chirp signal of inspiralling point masses very well before the dynamical interaction of the compact objects sets in. The final plunge of the two neutron stars produces maxima of the wave amplitude, the ongoing wave emission after the merging reflects the oscillations and the ringing of the massive remnant. The detailed structure of the signal during this phase depends on the assumed neutron star spins. If the remnant collapses to a black hole, this emission would be cut off.

For BH+NS mergers significant emission continues for a much longer time than predicted by the point-mass approximation, especially in case of $5\,\mathrm{M}_\odot$ and $10\,\mathrm{M}_\odot$ black holes where the neutron star survives the first approach, although it loses a major fraction of its mass to the black hole. The emission decreases to a negligible level once the neutron star is torn apart and its gas forms an accretion torus around the black hole. Maximum wave amplitudes rh are between $\sim 6\times10^4$ cm and $\sim 30\times10^4$ cm (Table 3).

6. Conclusions

Our three-dimensional hydrodynamical simulations of NS+NS and BH+NS merging, although basically Newtonian, allow for some interesting conclusions on potentially observable implications. We find that during the dynamical phase of the merging gas with a mass between $\sim 10^{-4}\,\mathrm{M}_\odot$ and several $10^{-2}\,\mathrm{M}_\odot$ may be ejected from the system and may become unbound. The exact amount depends sensitively on the neutron star spin(s) and on the mass of the black hole. The ejected gas may contribute to the chemical composition of the interstellar gas at a significant level. The nuclear composition of this gas has to be determined by detailed calculations of radioactive decays and possible r-processing. First interesting results have been obtained (Freiburghaus et al. 1999), but more work and more models are necessary. The ejection of radioactive material might also produce transient visible radiation, which could be observed in distant galaxies (Li & Paczyński 1998).

A detection of gravitational waves from the final, dynamical phase of the coalescence of NS+NS and BH+NS systems would yield rich information about the masses of the compact objects, their radii and the equation of state of neutron star matter. The upcoming km-scale interferometers have a chance to make such a ground-braking measurement, although estimates of the probability are very uncertain due to the observationally undetermined rates of mergers and many unknows in theoretical rate predictions. In addition, the sensitivity of experiments like LIGO is maximal around 100 Hz, and is worse by about a factor of 10 at 1000 Hz. The signal from the final plunge might be observable with LIGO only to a distance of $\sim 1\,\mathrm{Mpc}$, and with the advanced LIGO instrument only out to $\sim 10\,\mathrm{Mpc}$.

Whereas gravitational waves trace the geometry and mass distribution of the coalescing compact objects and the dynamics of the merging process, neutrinos can provide us with information about the thermodynamics of the gas. The emission of MeV neutrinos from NS+NS or BH+NS merger events could be comparable in energy to the neutrino signal from a supernova (in particular, if the NS+NS merger remnant does not collapse to a black hole quickly). Nevertheless, a direct measurement of these neutrinos is extremely unlikely, because the most optimistic estimates expect only one event in our Galaxy within 10^4 years, more than 100 times less frequent than core-collapse supernovae. Measuring the MeV neutrinos from extragalactic mergers will not be possible in the near future. If the catastropic destruction of NS+NS or BH+NS systems is associated with the production of a gamma-ray burst, however, high-energy in the 100 TeV range (Waxman & Bahcall 1997) and even ultra high-energy ($\sim 10^{18}$ eV) neutrinos (Waxman & Bahcall 2000) might be produced, which could lead to events in future km^3 detectors like AMANDA in the Antarctica.

We explored the possibility of powering a GRB by neutrino-antineutrino annihilation in the vicinity of the black hole, which accretes matter after the merging of the compact objects. Typical torus masses were found to be several tenths of a solar mass, with accretion rates of a few solar masses per second. The lifetime of the accretion disk might therefore be fractions of a second. During this time neutrinos could deposit an energy up to $\sim 10^{51}$ erg in a $e^{\pm}$ plasma cloud in the baryon-poor funnel above the poles of the black hole. Currently it is not clear how much these estimates may be affected by different properties of the accretion torus in a general relativistic simulation and by the rotation of a Kerr black hole. A possibly ultrarelativitically expanding jet would not be strongly collimated, but opening half-angles of several 10 degrees could increase the equivalent isotropic energy inferred by an observer in jet direction to values of several 10^{52} erg. The observable GRBs would probably have a hard spectrum and would be luminous above average (because of high $\nu\bar{\nu}$ energy deposition rates and not very large cosmological redshift), but would be of the short-duration type and less energetic than the long bursts. If the jet has to clean the axial funnel from baryons before maximal Lorentz factors are reached, a softer precursor to the actual GRB may be possible. Since the gas densities in the merger environment are low, the occurrence of afterglows seems unlikely, but matter, ejected during the merging or from the accretion torus by a neutrino-driven wind or by magnetic field effects might lead to associated emission at other wavelengths.

Very important questions cannot be satisfactorily answered by our current models but require further, preferably general relativistic simulations. Does the remnant of a NS+NS merger collapse to a black hole and if so, when does it collapse? Is the ejection of mass found in Newtonian models also present in case of the stronger relativistic gravity? How much mass ends up in an accretion torus around the black hole in this case? How does general relativity change the properties, neutrino emission and neutrino-antineutrino annihilation of the accretion disk? What are the lifetime of the accretion torus and how much energy is emitted by neutrinos or released by magnetic fields? Can a baryon-poor outflow form along the rotation axis and if so, how strong is the collimation of such a pair-plasma jet? What are the effects of a rapid rotation of the black hole? Do Kerr effects raise the efficiency of energy conversion from accretion to neutrinos and further to $e^{\pm}$ plasma? These questions have only been touched by current investigations and much more work is desirable. We have started to take a next, small step by using a pseudo-Newtonian (Paczyński & Wiita 1980) potential for the black hole in BH+NS systems, which allows us to roughly include the effects due to the existence of an innermost stable circular orbit. Using the description by Artemova, Bjoernsson, & Novikov (1996) we also consider the influence of the Kerr character of the black hole on the radius of the innermost stable orbit.

Acknowledgements

HTJ and MR would like to thank the organizers for an exciting and perfectly managed conference. Work on this project was supported by the U.K. PPARC as Advanced Fellow for MR and by the Deutsche Forschungsgemeinschaft on grant "Sonderforschungsbereich 375 für Astro-Teilchenphysik" for HTJ. We thank T. Eberl for running the BH+NS merger simulations as work for his Diploma Thesis. The calculations were performed at the Rechenzentrum Garching of the Max-Planck Gesellschaft.

References

Artemova, I.V., Bjoernsson, G., & Novikov, I.D. 1996, ApJ, 461, 565
Balberg, S., & Shapiro, S.L. 2000, astro-ph/0004317
Baumgarte, T.W., & Shapiro, S.L. 1998, ApJ, 504, 431
Baumgarte, T.W., Shapiro, S.L., & Shibata, M. 2000, ApJ, 528, L29
Berger, M.J. 1987, J. Numer. Anal., 24, 967
Berger, M.J., & Colella, P. 1989, J. Comput. Phys., 82, 64
Berger, M.J., & Oliger, J. 1984, J. Comput. Phys., 53, 484
Blanchet, L., Damour, T., & Schäfer, G. 1990, MNRAS, 242, 289
Blandford, R.D., & Znajek, R.L. 1977, MNRAS, 179, 433
Blinnikov, S.I., Novikov, I.D., Perevodchikova, T.V., & Polnarev, A.G. 1984, Sov. Astron. Lett., 10, 177
Bombaci, I., & Datta, B. 2000, ApJ, 530, L69
Bulik, T., Belczynski, K., & Zbijewski, W. 1999, MNRAS, 309, 629
Colella, P., & Woodward, P.R. 1984, J. Comput. Phys., 54, 174
Duez, M.D., Baumgarte, T.W., & Shapiro, S.L. 2000, gr-qc/0009064
Eberl, T. 1998, Diploma Thesis, Technical University Munich

Eichler, D., Livio, M., Piran, T., & Schramm, D.N. 1989, Nature, 340, 126
Freiburghaus, C., Rosswog, S., & Thielemann, F.-K. 1999, ApJ, 525, L121
Fryer, C.L., Woosley, S.E., & Hartmann, D. 1999, ApJ, 526, 152
Gondek, D., Haensel, P., & Zdunik, J.L. 2000, astro-ph/0012541
Heiselberg, H., & Pandharipande, V. 2000, Ann. Rev. Nucl. Part. Sci., 50, 481
Hulse, R.A., & Taylor, J.H. 1975, ApJ, 195, L51
Janka, H.-T., & Ruffert, M. 1996, A&A, 307, L33
Janka, H.-T., Eberl, T., Ruffert, M., & Fryer, C.L. 1999, ApJ, 527, L39
Kalogera, V., & Lorimer, D.R. 2000, ApJ, 530, 890
Klose, S. 2000, astro-ph/0001008
Kluźniak W., & Ruderman, M. 1998, ApJ, 505, L113
Kobayashi, S., & Sari, R. 2000, astro-ph/0101006
Lamb, D.Q. 2000, astro-ph/0005028
Lattimer, J.M., & Prakash, M. 2000a, Phys. Rept., 333–334, 121
Lattimer, J.M., & Prakash, M. 2000b, astro-ph/0002232
Lattimer, J.M., & Schramm, D.N. 1974, ApJ, 192, L145
Lattimer, J.M., & Schramm, D.N. 1976, ApJ, 210, 549
Lattimer, J.M., & Swesty, F.D. 1991, Nucl. Phys., A535, 331
Lattimer, J.M., Mackie, F., Ravenhall, D.G., & Schramm, D.N. 1977, ApJ, 213, 225
Lee, W.H. 2001, astro-ph/0101132
Lee, W.H., & Kluźniak, W. 1999a, ApJ, 526, 178
Lee, W.H., & Kluźniak, W. 1999b, MNRAS, 308, 780
Li, L.-X., & Paczyński, B. 1998, ApJ, 507, L59
Li, L.-X., & Paczyński, B. 2000, ApJ, 534, L197
Lipunova, G.V., & Lipunov, V.M. 1998, A&A329, 29
Mao, S., Narayan, R., & Piran, T. 1994, ApJ, 420, 171
Meyer, B.S. 1989, ApJ343, 254
Mitra, A. 2000, astro-ph/0010311
Narayan, R., Piran, T., & Shemi, A. 1991, ApJ, 379, L17
Otsuki, K., Tagoshi, H., Kajino, T., & Wanajo, S. 2000, ApJ, 533, 424
Paczyński, B. 1991, Acta Astronomica, 41, 257
Paczyński, B., & Wiita, P.J. 1980, A&A, 88, 23
Qian, Y.-Z., & Woosley, S.E. 1996, ApJ, 471, 331
Rosswog, S., Davies, M.B., Thielemann, F.-K., & Piran, T. 2000, A&A, 360, 171
Rosswog, S., Liebendörfer, M., Thielemann, F.-K., Davies, M.B., Benz, W., & Piran, T. 1999, A&A341, 499
Ruffert, M. 1992, A&A, 265, 82
Ruffert, M., & Janka, H.-T. 1998, A&A, 338, 535
Ruffert, M., & Janka, H.-T. 1999, A&A, 344, 573

Ruffert, M., Janka, H.-T., & Schäfer, G. 1996, A&A, 311, 532

Ruffert, M., Janka, H.-T., Takahashi, K., & Schäfer, G. 1997, A&A, 319, 122

Shibata, M., & Uryū, K. 1999, astro-ph/9911058

Sumiyoshi, K., Yamada, S., Suzuki, H., & Hillebrandt, W. 1998, A&A, 334, 159

Sumiyoshi, K., Suzuki, H., Otsuki, K., Terasawa, M., & Yamada, S. 2000, PASJ, 52, 601

Thorsett, S.E., & Chakrabarty, D. 1999, ApJ, 512, 288

Uryū, K., Shibata, M., & Eriguchi, Y. 2000, gr-qc/0007042

Usov, V.V. 1994, MNRAS, 267, 1035

Waxman, E., & Bahcall, J.N. 1997, Phys. Rev. Lett., 78, 2292

Waxman, E., & Bahcall, J.N. 2000, ApJ, 541, 707

Weber, F. 1999, Pulsars as Astrophysical Laboratories for Nuclear and Particle Physics (Bristol: IOP)